



# Improved electrocatalytic activity of carbon materials by nitrogen doping



Awan Zahoor<sup>a,b</sup>, Maria Christy<sup>b</sup>, Yun Ju Hwang<sup>b</sup>, Yi Rang Lim<sup>b</sup>,  
Pil Kim<sup>a,b</sup>, Kee Suk Nahm<sup>a,b,\*</sup>

<sup>a</sup> Department of Semiconductor and Chemical Engineering, Chonbuk National University, Jeonju 561-756, Republic of Korea

<sup>b</sup> R&D Education Center for Fuel Cell Materials & Systems, Chonbuk National University, Jeonju 561-756, Republic of Korea

## ARTICLE INFO

### Article history:

Received 10 April 2013

Received in revised form

12 September 2013

Accepted 23 September 2013

Available online 4 October 2013

### Keywords:

Nitrogen doping

Electrocatalyst

Nitrogen doped carbons

Oxygen reduction reaction

## ABSTRACT

The metal-based catalysts have been playing a major role in various industrial processes, whereas carbon based nanomaterials have recently been demonstrated to be promising metal-free alternatives for low cost catalytic processes. The doping of nitrogen in carbon and the electrocatalytic properties of the nitrogen doped carbon for oxygen reduction reactions are investigated in this article. We propose a simple method for doping nitrogen in various carbon materials like carbon black and ketjen black, and comparatively studied their physical and electrochemical characteristics. Raman and XPS analyses show significant peak shifts of their characteristic peaks caused by nitrogen doping on the surface of carbon materials. N-doped carbons show higher surface area in Brunauer, Emmett and Teller surface area analysis and more porous structure than undoped carbons in scanning electron microscope images. The N-doped sample was also ball milled to study the surface properties. All samples, i.e. undoped, N-doped and N-doped ball-milled carbons were compared for electrocatalytic activity by cyclic voltammetry and oxygen reduction reaction measurements. Nitrogen doped carbons exhibit better electrocatalytic activity with high mass activity and positive shift of peak potential than undoped samples with electron transfer number of 3.6 close to that of commercial Pt/C.

© 2013 Elsevier B.V. All rights reserved.

## 1. Introduction

The oxygen reduction reaction (ORR) at the cathode in fuel cells and lithium air batteries has attracted particular attention because it is an important process to control the cell performance [1–3]. In alkaline media, the most commonly used electrode is still uncatalyzed carbon, such as carbon–PTFE gas diffusion electrode or composite electrode made of graphite/teflon/carbon black. However, an electrocatalyst is essential for the effective adsorption of O<sub>2</sub> on the carbon electrodes. So it is important to find a suitable electrocatalyst for improved ORR performance [4–6].

In the past few years, considerable progress has been made in the understanding of ORR and at present platinum (Pt) and its alloys are considered to be highly electrocatalytic [7,8]. But even with Pt and other noble metal catalysts, ORR shows slow kinetics which is one of the main limiting factors for fuel cells and lithium air batteries. The major drawback of Pt based cathode materials is that they tend to be inactivated by carbon monoxide (CO) poisoning and by

agglomeration in addition to its cost and scarcity [9]. Therefore it is a great challenge to find out an alternative non-noble electrocatalysts for the cathode side of the fuel cells and metal batteries to replace Pt. There have been intensive research going on to replace suitable non-Pt based catalysts that exhibit similar activity of Pt, [10–12] and the progress has been reviewed elsewhere [13]. Meanwhile, in the last few decades, numerous studies [10–14] have been devoted to find alternative non-noble electrocatalysts like metal N<sub>4</sub> macrocycles; such as Fe<sup>+</sup> and Co<sup>+</sup> porphyrins and phthalocyanines, due to their high activity in the ORR.

Carbon materials have been widely used in heterogeneous catalytic reactions. For electro-catalysis application, high surface area carbons such as ketjen black (KB) and Vulcan carbon have also been used as supports because they are beneficial in terms of providing electronic conductivity and a high dispersion of metal catalysts [15,16]. The sp<sup>2</sup> carbon materials have abundant free flowing π electrons, which make them potential catalysts for reactions needing electrons, such as ORR. However, these π electrons are too inert to be used directly in ORR. In case of N-doped electron-rich carbon nanostructures, the carbon π electrons can be activated by conjugating with the lone-pair electrons from N dopants; thus, O<sub>2</sub> molecules get reduced on the positively charged carbon atoms neighboring nitrogen [17–23]. A wide variety of nanostructured, nitrogen-containing carbon materials like nanotubes, nanobells,

\* Corresponding author at: Department of Semiconductor and Chemical Engineering, Chonbuk National University, Jeonju 561-756, Republic of Korea.  
Tel.: +82 63 270 2311.

E-mail address: [nahmks@jbnu.ac.kr](mailto:nahmks@jbnu.ac.kr) (K.S. Nahm).

nanospheres and nanofibres [23–27], and layered sheets [19] etc., synthesized by various methods, such as chemical vapor deposition and sputtering techniques, have been investigated as ORR electrocatalysts.

Nitrogen doping of carbon materials can be achieved by several techniques [23,28]. Generally the techniques can be classified into two typical methods. In-situ doping is carried out during the synthesis of carbons, whereas post doping through post-treatment of pre-formed carbon nanostructures. In the former method, the in-situ nitrogen doping in CNTs or CNFs is generally achieved by decomposition of nitrogen containing hydrocarbons over metal catalyst particles such as Fe, Co, Ni and Cu. This can be achieved by various techniques such as, arc-discharge, laser ablation, chemical vapor deposition or thermal treatment [29–32]. But the presence of metal impurities gives a negative effect on the ORR because the impurities are not completely eliminated. To prepare similar CN<sub>x</sub> materials without involvement of metal particles, template method is also investigated. However, all those processes commonly require high energy consumption, expensive hardware and multistep processes, which are mostly responsible for high cost of manufacturing nitrogen doped carbon nanostructures and thus limit their practical applications. Recently, Lee et al. [33] employed low temperature microwave-assisted hydrothermal method to synthesize N-doped RGO and observed that N-doped RGO showed better property in their capacitor application owing to the presence of N-containing functional groups which increase the electronic charge density of graphene. The same authors also synthesized porous carbons at different temperatures through direct carbonization of N-containing precursor [34]. In the work, they reported that the N doped carbon prepared at higher temperature yields good electrocatalytic activity for the four electrons ORR.

In the latter method, the carbon material is subjected to heat treatment in a nitrogen containing atmosphere (NH<sub>3</sub> plasma, N-ion implantation, etc.) [26,35]. Post doping of carbon nanomaterials often leads to surface functionalization only without altering their bulk properties [36–38]. Different literatures [39,40] have confirmed that that ammoxidation or post doping mechanism is an easy process that can be used for the preparation of carbon electrodes that give high performance in electrochemical capacitors. Liu et al. [41] and Kichambare et al. [42] have also observed a significant increase in the specific area of the N doped carbons by post doping method in ordered carbon materials. Very recently, Yang et al. [43] proposed a powerful post doping technique for fabricating N-doped graphene at 900 °C and they have reported high electron transfer number of 3.93 and better electrocatalytic activity for ORR.

After careful analysis of various doping techniques, in this work, we doped various carbon materials with nitrogen by using post doping technique. Post doping technique is one of the promising methods for N doping in carbonaceous materials. We have slightly modified the previously reported thermal treatment methods. Our process involves a simple pretreatment process with HNO<sub>3</sub> followed by the reaction of NH<sub>3</sub> and N<sub>2</sub> gas in quartz tube reactor. This method is very cheap, facile, (solvent-, catalyst-, and template-free) easy to handle and subjective to increased scalability. Nitrogen doping significantly alters the morphology of the carbon materials and the N doped carbons show better catalytic activity for ORR.

## 2. Experimental methods

### 2.1. Pretreatment of carbon materials

Commercial carbons such as carbon black (CB) (acetylene) and KB (EC 600JD) were purchased and used for the experiment. The carbon samples were pretreated before nitrogen doping.

**Table 1**  
Names and symbols of the carbon samples used.

Carbons	Pure carbons	Nitrogen doped carbons	Ball milled and nitrogen doped carbons
Ketjen black	KB	NKB	MN KB
Carbon black	CB	NCB	MN CB
Carbon black + Ketjen black (blend)	B	NB	MN B

All the carbon materials CB, KB and B (Blend, blend of KB and CB) were pretreated with HCl to remove any unwanted impurities and to get better N-doping. The detailed process is as follows: The KB and CB carbon were washed with 6 M HCl for 24 h to remove metal impurities. The carbon materials were then rinsed several times with de-ionized (DI) water to remove chlorides and other impurities. The carbon materials were ball milled in high energy ball miller (Fritscher, Germany) for homogeneity.

### 2.2. Nitrogen doping

N-doped carbon materials were prepared at elevated temperatures as reported in previous literatures with little modifications [44,45]. The pretreated carbon was first refluxed with 70% HNO<sub>3</sub> in 100 ml flask and then heated at 378.15 K overnight. After cooling down, carbon powders were washed repeatedly by DI water followed by drying in an oven at 100 °C for 12 h. The dried materials were then treated with NH<sub>3</sub> and N<sub>2</sub> gas in quartz tube reactor at 900 °C at the rate of 5 °C/min for 100 min. The samples were again washed with boiling water to remove undesirable impurities and then kept in nitrogen atmosphere at 400 °C for 5 h. The CB and KB samples were separately studied with and without N-doping.

### 2.3. Characterizations

The morphological and crystallographic characteristics of all the carbon materials were examined by field emission scanning electron microscopy (FESEM), transmission electron microscopy (TEM) and X-ray diffraction (XRD) spectroscopy. The surface area analysis was carried out by Brunauer-Emmett-Teller (BET) surface areas analysis method. X-ray photoelectron spectroscopy (XPS), Fourier transform infrared (FTIR) spectroscopy and Raman spectroscopy were employed to examine the chemical composition and nitrogen doping. Cyclic voltammetry (CV) and rotating ring-disk electrode (RRDE) techniques were used to study electrocatalytic properties of the materials. All the materials characterization techniques including physical and electrocatalytic properties analysis are given separately in supporting material.

For a clear understanding all the prepared samples are categorized with their symbols in Table 1. Hereafter the samples will be referred by the respective symbols.

## 3. Results and discussion

### 3.1. Physical characteristics

FESEM measurements were taken to study the morphology of N doped samples. The FESEM image of undoped, N doped and 5 h ball milled (MN doped) carbon materials are shown in Fig. 1. All the samples observed by FESEM show no particular shape. The commercially obtained undoped carbon materials, i.e. KB and CB seem to have some clustered structures (secondary carbon particles) because of the agglomeration of primary carbon particles. They also show a random size distribution. Nitrogen doped samples, i.e. NKB, NCB and NB shows similar structures with no particular shape but uniform distribution of particles size than undoped carbons, which

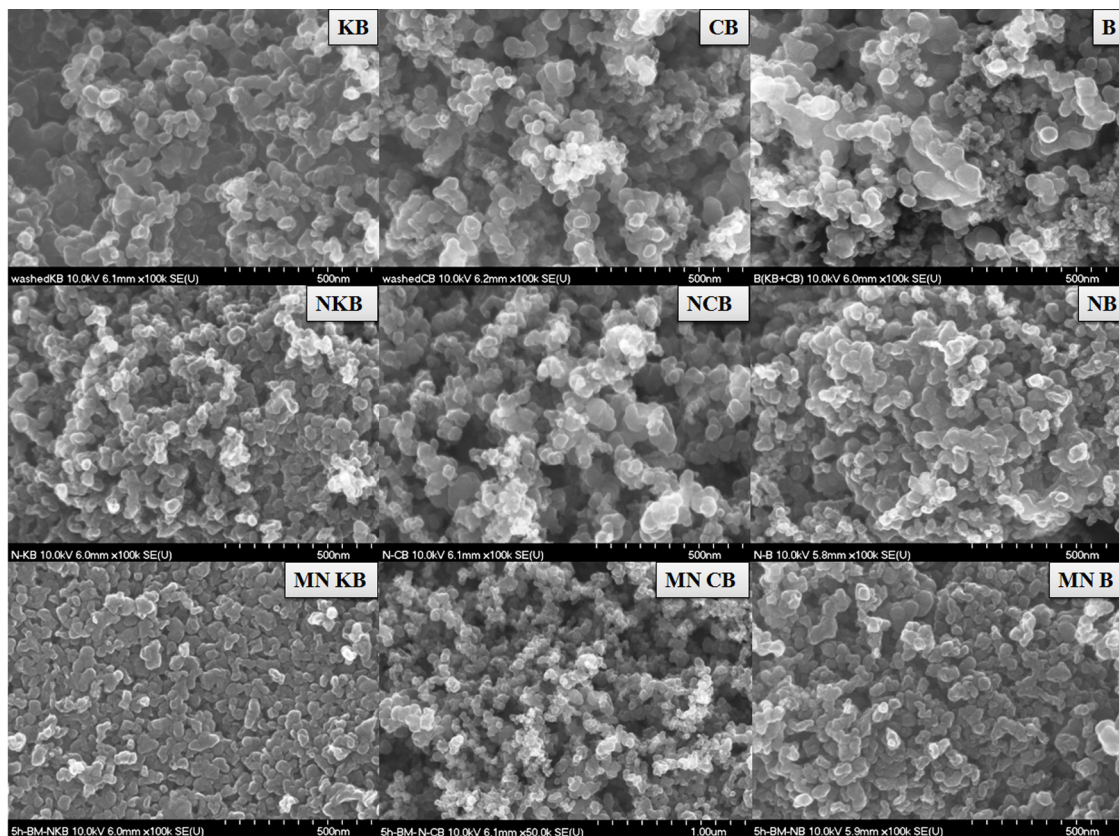


**Fig. 1.** FESEM images of undoped, N-doped and ball milled N-doped carbon materials.

indicates that nitrogen atoms are introduced into the carbon network [42]. After ball milling all the carbon materials, i.e. MN KB, MN CB and MN B show more uniform distribution with slight reduction in particle size. The average size of all the particles is in the range of 50–200 nm. For a clear insight on the carbon structures, TEM images were observed. All the TEM and HRTEM images of undoped and N doped carbons are given in Figure S1(supplementary information).

Fig. 2 shows the XRD patterns of undoped and N-doped carbon materials. The XRD spectra of all carbons reflect one pronounced peak around 23° and a weak peak at 44° corresponding to the (0 0 2) and (1 0 0) planes of graphite, respectively. The reflection (0 0 2) around 23° indicates the presence of a small domain with parallel stacking of graphene sheets, while the reflection (1 0 0) around 44° is attributed to the fibrous/spherical structures formed by  $sp^2$  hybridized carbons [42,46]. However, the diffraction peaks of nitrogen doped carbon materials is slightly shifted to higher  $2\theta$  values than those of undoped carbon materials due to the incorporation of nitrogen in the carbon. There was no observable shift in the (0 0 2) plane [46,47]. High energy ball milling of carbon materials can reduce the average sizes of the particle from the  $\mu\text{m}$  regime down to some nm. As it can be seen in Fig. 2, all the ball milled nitrogen doped materials have higher intensity at (0 0 2) reflection, in other words, milling the carbon materials leads to significant

ultra-micro porosity in the carbon materials which is quite evident from Table 2.

In order to analyze the surface area and pore properties, BET analysis was carried out and the detailed BET data for the undoped and N-doped carbon materials are given in Table 2. BET analysis is based on the adsorption of  $N_2$  gas on a material surface. From Table 2, it is clear that all the carbon materials exhibit higher specific surface area after N doping. The table also shows some increase in pore volume and pore size after nitrogen doping. During the preparation process of N-doped carbon materials, nitrogen atoms substitute some carbon atoms that are located on the reactive edge [48] and ammonia also reacts with carbon to form hydrogen cyanide and hydrogen ( $C + NH_3 = HCN + H_2$ ). This process consumed some carbon making the material more porous, resulting in the higher specific surface area, pore volume and pore size. Similar results have been reported by different researchers. For example, Liu et al. studied the N doping of ordered carbon materials by post heat treatment [41] and observed the increase of the specific surface area from  $832 \text{ m}^2 \text{ g}^{-1}$  for undoped to  $1132 \text{ m}^2 \text{ g}^{-1}$  for N-doped ordered porous carbon. Similarly, Kichambare et al. [42] also observed a significant increase in the specific surface area of N doped carbons than undoped carbons by post doping method. From Table 2, all the carbons show an increase in the surface area

**Table 2**

Detailed BET data of undoped, N-doped and ball milled N-doped carbon materials.

	KB	NKB	MN KB		CB	NCB	MN CB		B	NB	MN B	
			1 h	5 h			1 h	5 h			1 h	5 h
Surface area ( $\text{m}^2 \text{ g}^{-1}$ )	522.12	781.46	775.50	525.26	137.91	266.4	259.85	300.68	117.88	375.79	306.55	1002.4
Pore volume ( $\text{cm}^3/\text{g}$ )	0.79	1.38	1.68	0.87	0.25	0.48	0.69	0.85	0.10	0.38	0.83	2.85
Pore size (nm)	6.05	7.08	8.66	6.82	7.18	7.24	10.61	10.65	3.37	4.06	10.81	11.36

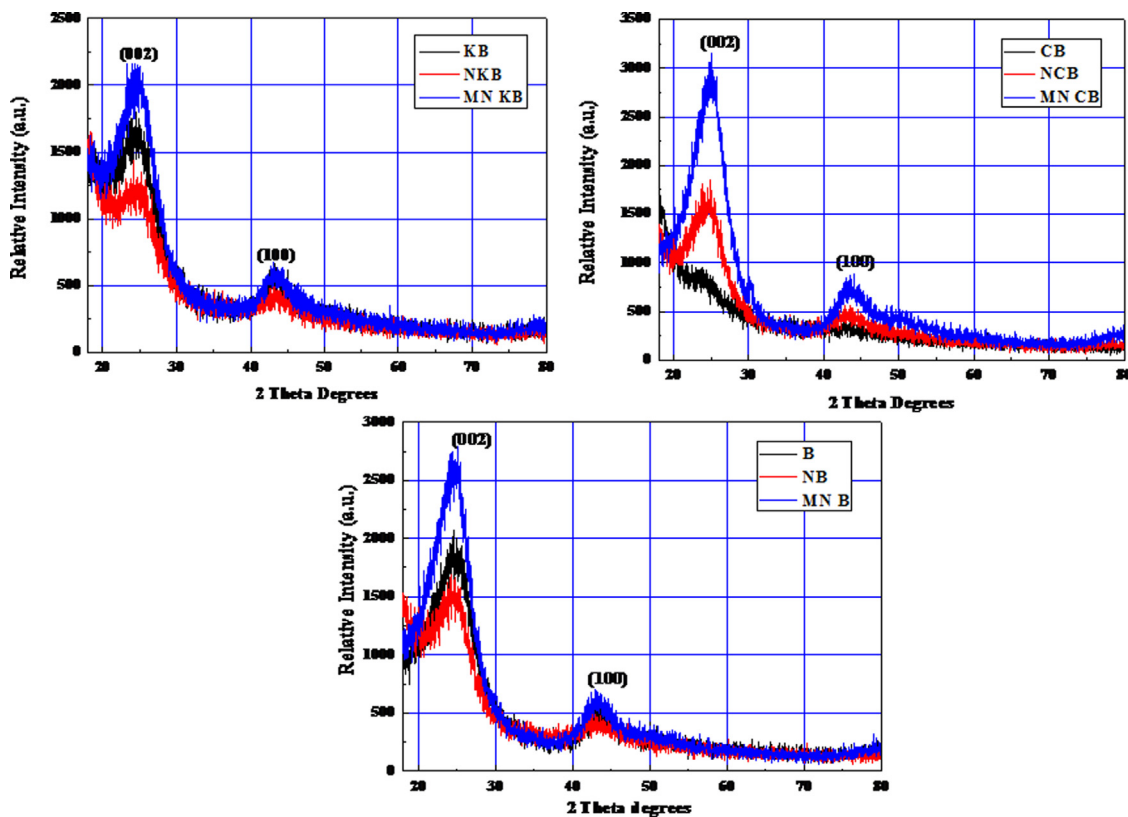


**Fig. 2.** XRD pattern of undoped, N-doped and ball milled N-doped carbons materials.

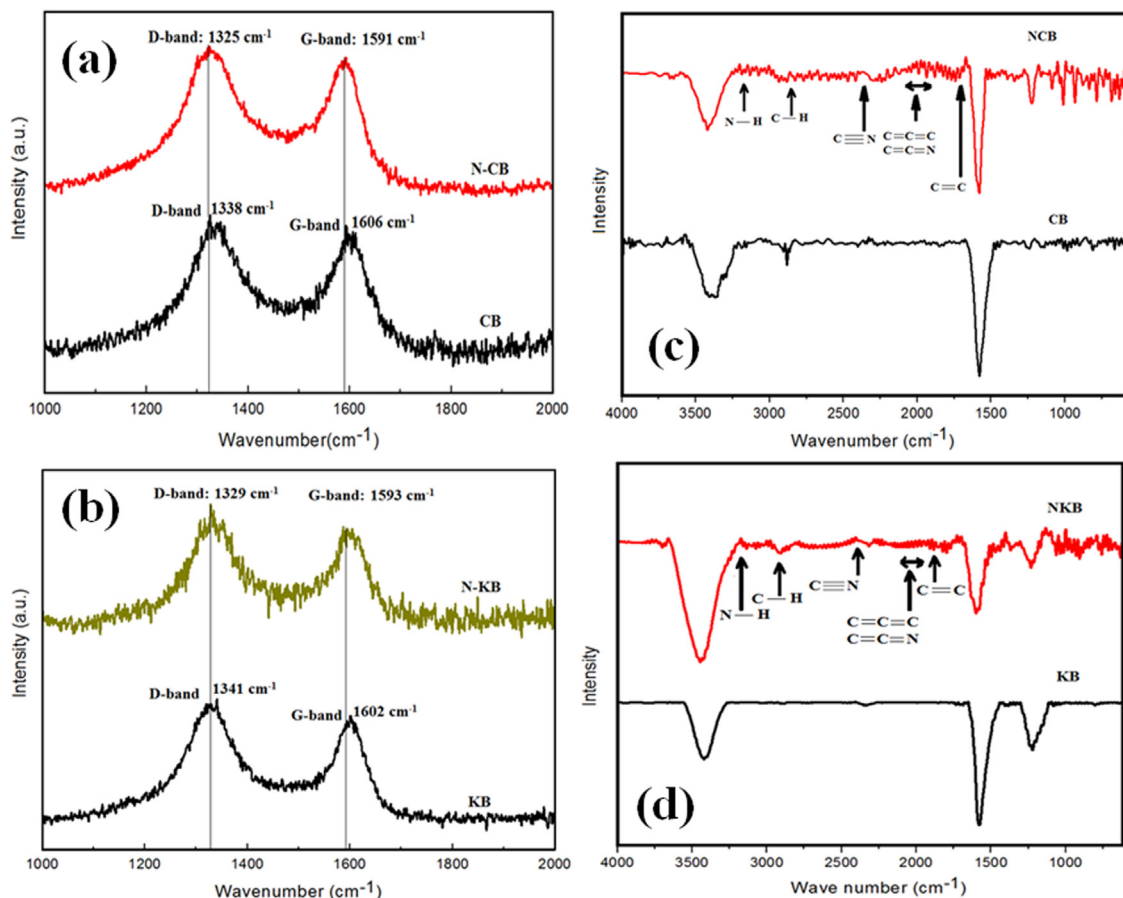


**Fig. 3.** Raman and FTIR spectra of undoped and N-doped carbons materials.

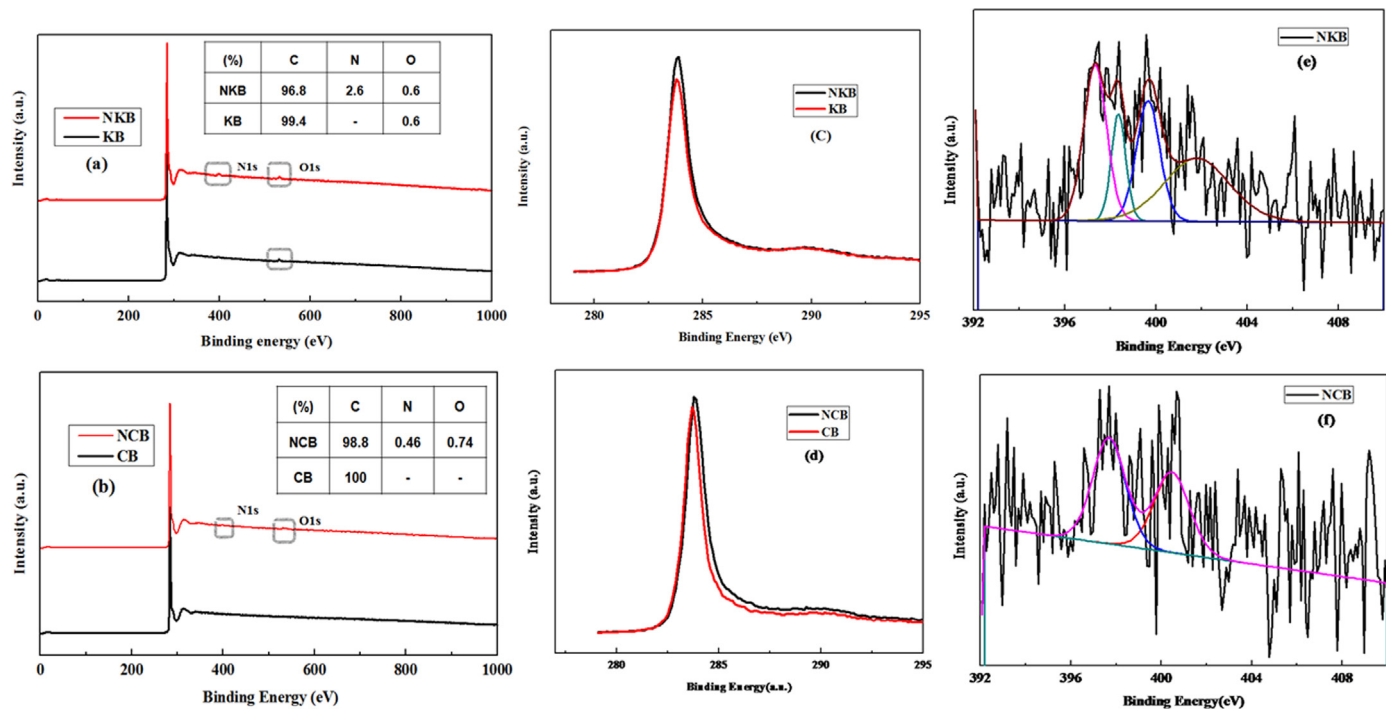


Fig. 4. XPS spectra of undoped and N-doped carbons materials.

on N doping and a further increase in the surface area upon ball milling for an hour. But, upon further ball milling for 5 h, the surface area almost decreases to its original value. This may be due to the change in surface properties of the material upon increased ball milling time. Similar dramatic surface area modification was also observed by Xiao et al. [49]. The  $\text{N}_2$  adsorption–desorption isotherms are also in consistent with this change in surface area and pore volume. The  $\text{N}_2$  adsorption–desorption isotherm and pore size distribution (details deduced in Table 2) for undoped and N-doped carbon materials are given in supporting material (Figures S2 and S3).

In order to identify the N doping, Raman spectroscopy analysis was carried out for the carbon samples. The Raman spectra show that NCBs has two distinct peaks at around  $1325$  and  $1591\text{ cm}^{-1}$  as seen in Fig. 3a which corresponds to the D band and G band, respectively. The D and G bands of the pristine CB show a shift of the peaks to  $1338\text{ cm}^{-1}$  and  $1606\text{ cm}^{-1}$ , respectively. Similar results were obtained for NKB from Fig. 3b, where the D and G bands of NKB are located at  $1329$  and  $1591\text{ cm}^{-1}$  and are shifted to  $1341$  and  $1602\text{ cm}^{-1}$  for pristine KB. This result obtained from our nitrogen doped carbons is similar to those of nitrogen-doped CNTs [47,50–52]. The G band related to the E2 g vibration mode of  $\text{sp}^2$  carbon domains explains the degree of graphitization, while the D band is associated with structural defects and partially disordered structures of the  $\text{sp}^2$  domains. From the Raman curves the intensity ratio of NCB is found to be  $I_{\text{D}}/I_{\text{G}} = 1.05$  which is higher than CB ( $I_{\text{D}}/I_{\text{G}} = 1.01$ ). NKB have the intensity ratio  $I_{\text{D}}/I_{\text{G}} = 1.1$ , which is again higher than pristine KB ( $I_{\text{D}}/I_{\text{G}} = 1.06$ ). The  $I_{\text{D}}/I_{\text{G}}$  ratios are larger for N-doped carbons due to the structural defects and edge plane exposure caused by heterogeneous nitrogen atom incorporation into the graphite layers present on the surface of N-doped carbon materials [50–52].

FTIR analysis was carried out for all the samples in order to investigate their chemical composition. FTIR spectra of N doped and undoped CB and KB are given in Fig. 3c and d, respectively. The broad, low intensity peaks between  $3743$  and  $3100\text{ cm}^{-1}$  are attributed to N–H stretches, which suggests the hydrogenation of

some of the nitrogen atoms. The broad, low intensity peaks between  $3100$  and  $2800\text{ cm}^{-1}$  are attributed to C–H stretches. The peak at  $2373\text{ cm}^{-1}$  is attributed to stretching vibration modes of isonitrile  $\text{C}\equiv\text{N}$  cyano terminal groups. The broad set of peaks between  $\sim 2100$  and  $1900\text{ cm}^{-1}$  are attributed to allene groups ( $\text{C}=\text{C}=\text{C}$ ) or ketamine groups ( $\text{C}=\text{C}=\text{N}$ ). The band located at  $1740\text{ cm}^{-1}$  corresponds to the  $\text{C}=\text{C}$  stretching vibration [53]. Due to the disordering of the graphite-like structure after introduction of nitrogen atoms into the carbon network, the sharp peaks in the CB and KB assigned to the graphitic  $\text{sp}^2$  carbon atoms shifts to higher intensities with narrow and intensive peaks which also confirms the N doping.

XPS analysis was carried out to investigate the chemical composition of undoped and N doped carbons. Fig. 4a–e shows the measured XPS spectra with elemental analysis data in the inset. The XPS spectra of NKB and NCB (Fig. 4a and b) show the presence of carbon and very small amount of nitrogen and oxygen. From the magnified spectra (Fig. 4c and d) it can be seen that the C1s spectrum of NKB and KB has a binding energy of  $283.9\text{ eV}$  and that of NCB and CB at  $284.2\text{ eV}$ , which are well consistent with  $\text{sp}^2$  graphitic carbon [54]. The binding energies of nitrogen and oxygen are observed at  $401.8$  and  $528.4\text{ eV}$ , respectively, regardless of the samples. However, only carbon and oxygen were detected in the undoped KB and only carbon was detected in undoped CB. Since all N doped samples shows N signal, this also confirms the successful N doping on carbon materials. There is a slight increase in the C–N peak intensity which is clearly seen from the magnified C1s spectra of NKB and NCB. This increase in the peak intensity is due to the presence of nitrogen functional group on the surface of the material [55]. For a clear understanding, elemental analysis data (inset table in Fig. 4a and b), is shown with different concentrations of nitrogen observed in NKB and NCB. Clearly, no traces of nitrogen can be found in undoped KB and CB. The surface nitrogen concentration in NKB and NCB is determined to be  $2.6$  and  $0.46\%$ , respectively. Fig. 4e and f shows the deconvoluted XP N1s spectra of the NKB and NCB samples. Fitting of the N1s spectra of NKB yields three different peaks at  $398.3\text{ eV}$ ,  $399.6\text{ eV}$  and  $401.8\text{ eV}$  which are attributed to the pyridinic nitrogen, pyrrolic-type nitrogen, and quaternary nitrogen, respectively.

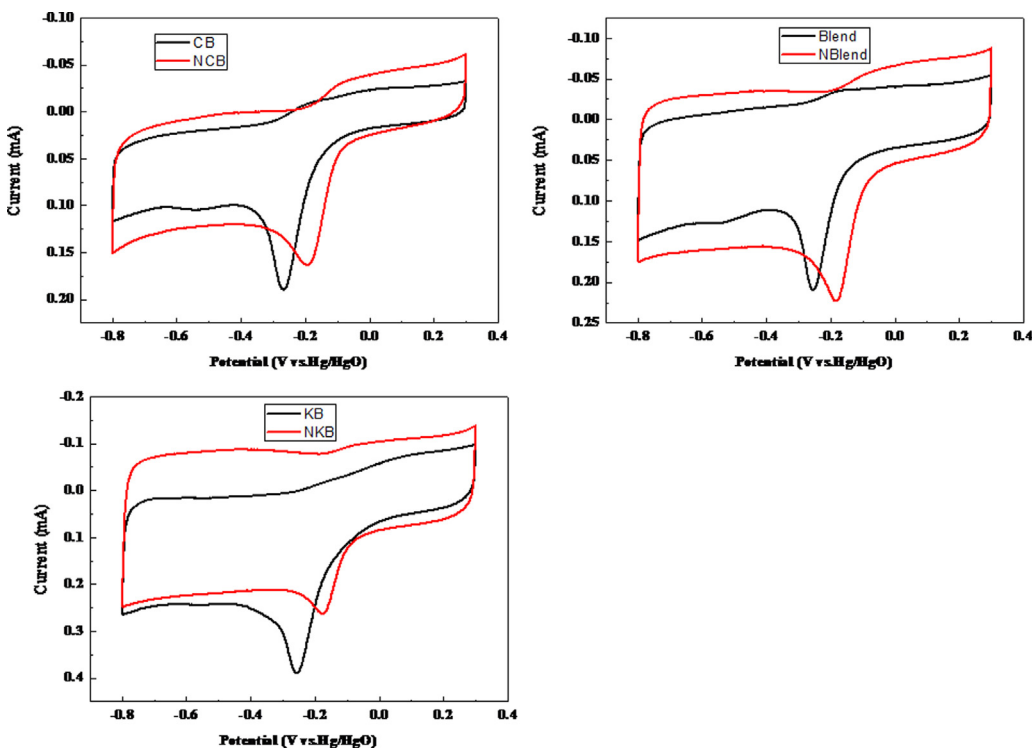


**Fig. 5.** Cyclic voltammograms of undoped and N-doped carbon materials in  $O_2$  saturated 0.1 M KOH solution at 5 mV/s.

For NCB only two peaks were observed at 397.9 eV and 400.4 eV which are attributed to the pyridinic and pyrrolic nitrogen, respectively. This again shows the successful N doping in our KB and CB carbons.

### 3.2. Electrocatalytic properties

Cyclic voltammetry and rotating ring-disk electrode (RRDE) technique were used to explain the electrocatalytic activity of N doped carbons toward the ORR. The catalytic activity of a catalyst to the ORR could be qualitatively estimated from the onset and reduction peak potentials in CV. Fig. 5 depicts cyclic voltammograms (CV) for  $O_2$  reduction on undoped and N-doped carbon materials in  $O_2$  saturated 0.1 M KOH electrolyte solution at a scan rate of 5 mV/s. For comparison, the CV for the  $O_2$  reduction with  $N_2$  saturated 0.1 M KOH electrolyte solution was also performed at the same scan rate and is given in Figure S4 in supporting material. All the undoped and N-doped carbons showed similar features under  $N_2$  saturated electrolyte solution with a small redox peak in between  $-0.30$  and  $-0.15$  V due to pseudocapacitive behavior of N doped carbons, which is similar to other observations [53]. From Fig. 5 under  $O_2$  purged solutions, however, MNKB and MN B show quasi rectangular voltammograms typical of high surface area carbons [48]. In the undoped samples, the electrochemical reduction occurs in two step processes with onset potential at  $-0.1$  and  $-0.5$ . The N doped carbon samples exhibit a significant positive shift of onset potential than undoped carbons. The onset potentials of MN KB and KB are  $-0.08$  and  $-0.11$ , respectively. The onset potentials of MNCB and CB are  $-0.09$  and  $-0.13$ , respectively, while those of MNB and B are  $-0.09$  and  $-0.15$ , respectively. It is clear from the figures that the onset potentials of N doped samples are less negative than undoped samples due to fast reaction kinetics and high transferred electron number per oxygen molecule. Owing to the fast reaction kinetics and positive shifted onset potential, N doped carbons proves to be highly electrocatalytic towards ORR [56].

For a clear understanding, we examined the effect of nitrogen doping in carbon materials on the ORR performance with linear sweep voltammograms (LSVs). The LSV was recorded in  $O_2$  saturated 0.1 M KOH at a scan rate of 5 mV/s over the electrode rotation rate of 1600 rpm, as shown in Fig. 6. For comparison, ORR was also performed on commercial 20 wt.% Pt/C under the same experimental conditions (Fig. 6). For each of the investigated materials, the onset potential and half wave potential (HWP) for ORR are given in Table 3. The onset potentials of 5 h MN CB, 5 h MN KB and 5 h MN B are  $-0.09$ ,  $-0.07$  and  $-0.07$  V, respectively, which are more positive than undoped CB, KB and B with HWP values of  $-0.25$  V,  $-0.23$  and  $-0.23$  V, respectively. Although the onset and half wave potentials of N doped samples are a little bit lower

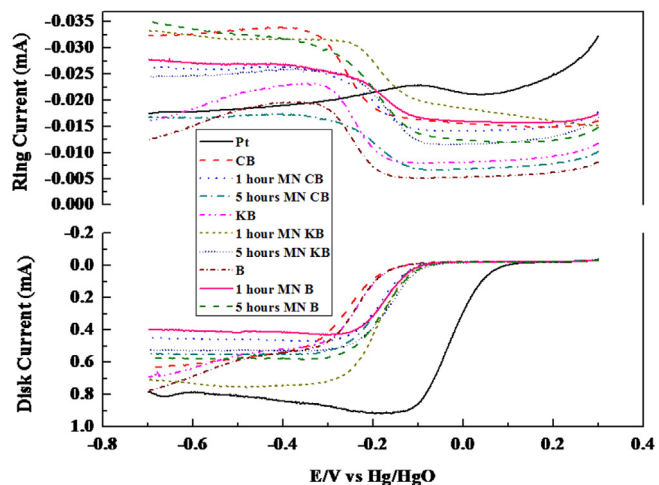


**Fig. 6.** Linear sweep voltammograms (LSV) of undoped and N-doped carbon samples in  $O_2$  saturated 0.1 M KOH electrolyte (scan rate: 5 mV/s); rotation rate: 1600 rpm.

**Table 3**

Onset potentials, limiting current and half wave potentials of different carbon samples (values derived from Fig. 5).

Sample no.	Sample	Onset potential (V)	Limiting current (mA)	Half wave potential (V)	No. of electron transfer ( <i>n</i> )
1	CB	-0.12	0.53	-0.25	3.4
2	1 h MN CB	-0.09	0.45	-0.18	3.4
3	5 h MN CB	-0.09	0.55	-0.18	3.6
4	KB	-0.13	0.69	-0.23	3.4
5	1 h MN KB	-0.08	0.70	-0.18	3.6
6	5 h MN KB	-0.07	0.52	-0.16	3.6
7	B	-0.12	0.53	-0.23	3.6
8	1 h MN B	-0.08	0.40	-0.17	3.3
9	5 h MN B	-0.07	0.58	-0.17	3.5
10	Pt/C	0.05	0.78	0.02	3.8

than those of Pt/C (which are 0.05 V and 0.02 V), the significant positive shift in the N doped carbons with respect to undoped carbons explicitly shows that N doped carbons are catalytically more active [57]. Similar results were reported by different researchers [42,58–60]. Stevenson et al. [61] reported the influence of nitrogen concentration in the N-doped carbons on the electronic, structural and electrochemical properties. They observed the increase in bulk electrical conductivity, work function, and the density of states at the Fermi level with the increased nitrogen doping in CNTs. Wang et al. [59] also investigated ammonia-treated ordered mesoporous carbons as catalytic materials for oxygen reduction reaction and found that the ORR activities were not induced by trace amount of metal species, but by the presence of active nitrogen species.

We have calculated the electron transfer number per oxygen molecule (*n*) during ORR from Fig. 6 by using the equation,  $n = 4I_D/(I_D + (I_R/N))$ , where  $I_D$ ,  $I_R$  and  $N$  are disk current, ring current and ring collection efficiency (here  $N=0.37$ ) respectively. The calculated *n* values of all the materials are included in Table 3. Basically, there are two proposed mechanisms for the ORR: (i) a direct four-electron transfer mechanism and (ii) a two-by-two electron (two steps) mechanism, which goes through a hydroperoxide intermediate ( $\text{HO}_2^-$ ) to complete the reaction [61]. In the second mechanism, the  $\text{HO}_2^-$  intermediate can undergo disproportionation reaction which prevents the second step reaction. Moreover, the base-stabilized hydroperoxide ( $\text{HO}_2^-$ ) can degrade the carbon support, catalyst, and/or membrane, resulting in poor ORR. Therefore, it is important to develop a bifunctional catalyst that promotes a direct four-electron mechanism. In our experiment, for N doped KB,CB and B, the electron transfer numbers, *n*, are found to be in the range of 3.4–3.6 (Table 3). This indicates that our prepared N doped carbon materials are suitable catalysts for the direct four electron mechanism in ORR. Lee et al. [34] has synthesized collagen derived N doped porous carbons for electrocatalytic production of  $\text{H}_2\text{O}_2$ . They synthesized the collagen derived N doped carbons at different temperatures and measured the electron transfer number (*n*) of the synthesized N doped carbons at different potentials. It is interesting to see that they observed the collagen derived N doped carbon has *n* value of 3.7 at 800 °C, close to 4, while at lower temperatures the samples exhibit *n* value close to 2. From the experiment, Lee et al. suggests that the sample with *n* = 3.7 possesses a great potential to be electrocatalysts for the direct four electron mechanism for ORR in the application of fuel cells and metal air batteries, whereas the sample with *n* values closed to 2.0 are considered as excellent electrocatalysts for the ORR to boost  $\text{H}_2\text{O}_2$  generation. Ma et al. [56] has also obtained electron transfer number (*n*) of 3.7 for nitrogen doped hollow carbon nanoparticles indicating that an efficient four-electron pathway is the dominant reaction mechanism during the electrochemical process. Moreover, Sheng et al. [52] evaluated the transferred electron number for pure and N doped graphene. The calculated *n* value was about 2.2–2.4 for pure graphene and 3.4–3.6 for N doped graphene, respectively. This reveals that the electrocatalytic process of N doped graphene is suitable for direct

four electron mechanism for ORR. So the N doped materials are proved to possess great potential to be applied as electrocatalysts in fuel cells and metal air batteries. Very recently, Yang et al. [43] has reported high electron transfer number of 3.93 and more, which are much higher *n* value than any other reports, including our work. They have synthesized nitrogen doped graphene sheets from a melamine employed graphene oxide mixture by covalent transformation. It is considered that GO exhibits excellent electrocatalytic properties than disordered carbons due to its superior structural and electrochemical characteristics such as high specific surface area, conductivity, and uniform porosity [19].

To check the durability and life span of the electrode material, we also measured cyclic voltammogram for all the N doped and undoped carbon materials for 10 cycles. All the samples gave steady and consistent features with not much change in the voltammograms given in Figure S5 (supporting material). The structural defects introduced by N-doping increase the amount of unsaturated carbon atoms and these atoms react with oxygen to form oxygen containing functional groups which enhances the ORR. The doped nitrogen with lone electron pair could provide additional negative charges which enhance the interaction between carbon structures and foreign molecules and increase the conductivity. This is ascribed to the conjugation effect of the nitrogen lone pair electrons on the nitrogen and graphene  $\pi$ -system. There are more defects after nitrogen doping, and the carbon atoms adjacent to nitrogen possess higher positive charge density, resulting in an enhanced adsorption of oxygen and reactive intermediates which enhances the ORR [57]. The significant positive shifts in reduction peak and onset potential in CV and LSV of ORR of N doped carbon samples imply that they are catalytically more active than the undoped carbon samples. The low ORR activity of undoped carbon samples may be due to the weak bonding of the intermediate oxygen reduction species and lower surface area [57].

The better performance of KB and B samples can be attributed to their high mesopore volume. After ball milling (Table 2) the pore volume and surface area of KB were reduced than that of their original values, respectively, which are similar to the previous observation [49]. This result clearly indicates a direct correlation between the mesopore volume and electrocatalytic activity of the carbon, especially when there is a large difference in pore volume between the carbon sources. In general, all the N doped carbons exhibit high electrocatalytic properties than undoped carbons. NKB and NB shows better electrocatalytic activity with high surface area, pore volume and pores size. Even though the N-doped carbon material exhibits lower ORR activity than commercial Pt/C, there is still a great possibility to improve the performance of N-doped carbons. This can be accomplished by modification of its electronic structure or by increasing the number of active sites through synthesis techniques by increasing in reaction time and reaction temperature.

The specific activity and mass activity of undoped and N-doped carbon samples with their kinetic currents at two different

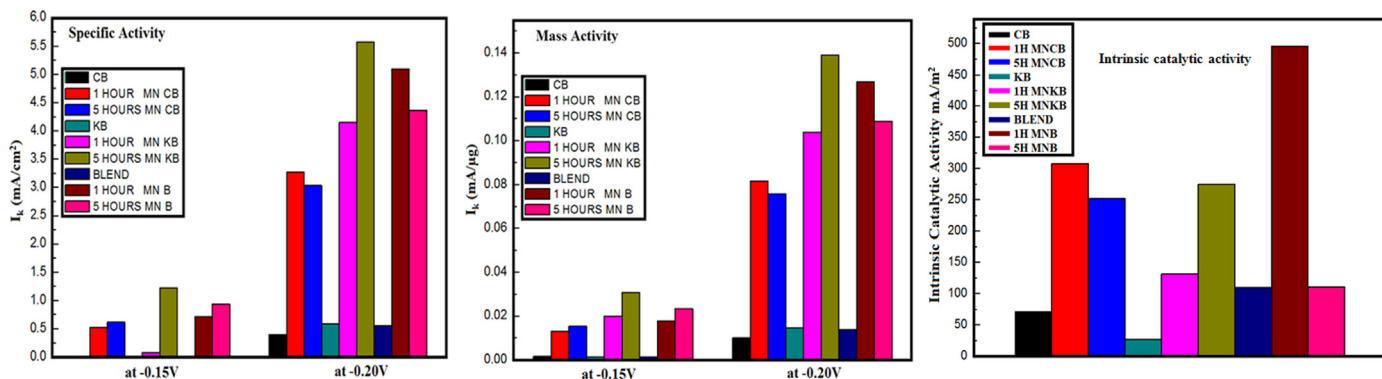


**Fig. 7.** Specific, mass and intrinsic catalytic activity of different carbon samples obtained at -0.15 and -0.20 V (vs. Hg/HgO; 0.1 KOH) derived from Fig. 6.

potentials -0.15 and -0.20 V are given in Fig. 7. The 5 h MN KB sample shows highest mass and specific activities in both cases. The N doped samples show better mass and specific activity compared to the undoped samples due to the incorporation of nitrogen onto the carbon matrix which favors the reactivity of the neighborly linked carbon atoms by alteration of the electronic structure [61,62]. The low activities of the undoped samples are due to their lower surface area. The intrinsic catalytic activity based on the surface area of catalysts is also given in Fig. 7. From the above results, it is seen that the increase in ORR activity is closely correlated to the N-doping, i.e. N-doped carbons exhibits better electrocatalytic activity. NKB of all carbon materials show high surface area and better electrocatalytic properties followed by NB. The high selectivity of nitrogen doped carbon toward ORR makes it a very promising electrocatalyst.

#### 4. Conclusion

N-doped carbon materials were synthesized by a post doping method and were characterized with various structural and electrochemical analytic techniques. The synthesized carbon materials show pure, mesoporous structures with nitrogen doping. NKB and NB carbon materials show higher surface area than undoped samples. The incorporation of nitrogen in the carbon plays an important role in the ORR process. The electrocatalytic activity for ORR significantly increases with N-doping comparable with commercial Pt/C. The N doping introduces structural defects and doped nitrogen with lone electron pairs provides negative charges. The carbon atoms adjacent to nitrogen with high positive charge density increase their interaction which results in the enhanced ORR activity. Among all the N-doped samples, NKB shows better physical and electrocatalytic characteristics.

#### Acknowledgements

This work was supported by the Human Resources Development program (NO. 20114030200060) of the Korea Institute of Energy Technology Evaluation and Planning (KETEP) grant funded by the Korea government Ministry of Trade, Industry and Energy. One of our authors Mr. Awan Zahoor is thankful to the NED University of Engineering & Technology, Pakistan, for their financial support rendered for his PhD.

#### Appendix A. Supplementary data

Supplementary data associated with this article can be found, in the online version, at <http://dx.doi.org/10.1016/j.apcatb.2013.09.043>.

#### References

- [1] C.B. Sarah, Platinum Met. Rev. 49 (1) (2005) 27–32.
- [2] F. Alcaide, E. Brillas, P.L. Cabot, J. Electrochem. Soc. 149 (2002) 64.
- [3] R.J. Taylor, A.A. Humffray, J. Electroanal. Chem. 64 (1975) 63.
- [4] J. Xu, W. Huang, R.L. McCreery, J. Electroanal. Chem. 410 (1996) 235.
- [5] Z.W. Zhang, D.A. Tryk, E.B. Yeager, in: S. Sarangapani, J.R. Akridge, B. Schumm (Eds.), Proceedings of the Workshop on the Electrochemistry of Carbon, The Electrochemical Society, Pennington, NJ, 1984, p. 158.
- [6] T. Nagaoka, T. Sakai, K. Ogura, T. Yoshino, Anal. Chem. 58 (1986) 1953.
- [7] J. Zhang, K. Sasaki, E. Sutter, R.R. Adzic, Science 315 (2007) 220.
- [8] H. Yano, J. Inukai, H. Uchida, M. Watanabe, P.K. Babu, T. Kobayashi, J.H. Chung, E. Oldfield, A. Wieckowski, Phys. Chem. Chem. Phys. 8 (2006) 4932–4939.
- [9] T.R. Ralph, M.P. Hogarth, Platinum Met. Rev. 46 (3) (2002) 117–135.
- [10] M. Lefèvre, E. Proietti, F. Jaouen, J.P. Dodelet, Science 324 (5923) (2009) 71–74.
- [11] R. Bashyam, P. Zelenay, Nature 443 (2006) 63–66.
- [12] G. Wu, K.L. More, C.M. Johnston, P. Zelenay, Science 332 (2011) 443–447.
- [13] A. Serov, C. Kwak, Appl. Catal. B: Environ. 90 (2009) 313–320.
- [14] F. Jaouen, J.P. Dodelet, J. Phys. Chem. C 113 (34) (2009) 15422–15432.
- [15] L.R. Radovic, F. Rodriguez-Reinoso, Carbon materials in catalysis, in: P.A. Thrower (Ed.), Chemistry and Physics of Carbon, vol. 25, Dekker, New York, 1997, pp. 243–358.
- [16] G.G. Wildgoose, C.E. Banks, R.G. Compton, Small 2 (2) (2006) 182–193.
- [17] K. Gong, F. Du, Z. Xia, M. Durstock, L. Dai, Science 323 (2009) 760.
- [18] Y.F. Tang, B.L. Allen, D.R. Kauffman, A. Star, J. Am. Chem. Soc. 131 (2009) 13200.
- [19] L. Qu, Y. Liu, J.Y. Baek, L. Dai, ACS Nano 4 (2010) 1321.
- [20] S. Chen, J.Y. Bi, Y. Zhao, L.J. Yang, C. Zhang, Y.W. Ma, Q. Wu, X.Z. Wang, Z. Hu, Adv. Mater. 24 (2012) 5593.
- [21] E. Yoo, J. Nakamura, H. Zhou, Energy Environ. Sci. 5 (2012) 6928.
- [22] D. Yu, Q. Zhang, L. Dai, J. Am. Chem. Soc. 132 (2010) 15127.
- [23] Y. Shao, J. Sui, G. Yin, Y. Gao, Appl. Catal. B: Environ. 79 (2008) 89–99.
- [24] M.S. Saha, R. Li, X. Sun, S. Ye, Electrochim. Commun. 11 (2009) 438–441.
- [25] E.G. Wang, J. Mater. Res. 21 (11) (2006) 2767–2773.
- [26] X. Zhou, Z. Yang, H. Nie, Z. Yao, L. Zhang, S. Huang, J. Power Sources 196 (2011) 9970–9974.
- [27] S. Maldonado, K.J. Stevenson, J. Phys. Chem. B 109 (2005) 4707–4716.
- [28] Y. Zhou, K. Neyerlin, T.S. Olson, S. Pylypenko, J. Bult, H.N. Dinh, T. Gennett, Z. Shao, R. O’Hayre, Energy Environ. Sci. 3 (2010) 1437–1446.
- [29] M. Glarup, J. Steinmetz, D. Samaille, O. Stephan, S. Enouz, A. Loiseau, S. Roth, P. Bernier, Chem. Phys. Lett. 387 (2004) 193–197.
- [30] M. Yudasaka, R. Kikuchi, Y. Ohki, S. Yoshimura, Carbon 35 (2) (1997) 195–201.
- [31] Y.J. Kim, Y. Abe, T. Yanagiura, K.C. Park, M. Shimizu, T. Iwazaki, S. Nakagawa, M. Endo, M.S. Dresselhaus, Carbon 45 (2007) 2116–2125.
- [32] L. Zhao, L.Z. Fan, M.Q. Zhou, H. Guan, S. Qiao, M. Antonietti, M.M. Titirici, Adv. Mater. 22 (2010) 5202–5206.
- [33] Y.H. Lee, K.H. Chang, C.C. Hu, J. Power Sources 227 (2013) 300–308.
- [34] Y.H. Lee, F. Li, K.H. Chang, C.C. Hu, T. Ohsaka, Appl. Catal. B: Environ. 126 (2012) 208–214.
- [35] X. Wang, X. Li, L. Zhang, Y. Yoon, P.K. Weber, H. Wang, J. Guo, H. Dai, Science 324 (5928) (2009) 768–771.
- [36] L. Jiang, L. Gao, Carbon 41 (2003) 2923–2929.
- [37] S.C. Roy, A.W. Harding, A.E. Russell, K.M. Thomas, J. Electrochim. Soc. 144 (1997) 2323–2328.
- [38] R.A. Sidik, A.B. Anderson, N.P. Subramanian, S.P. Kumaraguru, B.N. Popov, J. Phys. Chem. B 110 (2006) 1787–1793.
- [39] N.D. Kim, W.Y. Kim, J.B. Joo, S.G. Oh, P. Kim, Y. Kim, J. Yi, J. Power Sources 180 (2008) 671.
- [40] K. Jurewicz, K. Babel, A. Ziolkowski, H. Wachowska, M. Kozlowski, Fuel Process. Technol. 77–78 (2002) 191–198.
- [41] G. Liu, X. Li, P. Ganeshan, B.N. Popov, Appl. Catal. B: Environ. 93 (2009) 156–165.
- [42] P. Kichambare, J. Kumar, S.S. Rodrigues, B. Kumar, J. Power Sources 196 (2011) 3310.

- [43] S.Y. Yang, K.H. Chang, Y.L. Huang, Y.F. Lee, H.W. Tien, S.M. Li, Y.H. Lee, C.H. Liu, C.M. Ma, C.C. Hu, *Electrochim. Commun.* 14 (2012) 39–42.
- [44] M. Kawaguchi, S. Yagi, H. Enomoto, *Carbon* 42 (2) (2004) 345–350.
- [45] R.J.J. Jansen, H.V. Belkum, *Carbon* 33 (8) (1995) 1021–1027.
- [46] Y. Li, J. Wang, X. Li, J. Liu, D. Geng, J. Yang, *Electrochim. Commun.* 13 (7) (2011) 668.
- [47] S. Lim, S.H. Yoon, I. Mochida, D. Jung, *Langmuir* 25 (2009) 8268–8273.
- [48] P. Simon, Y. Gogotsi, *Nat. Mater.* 7 (11) (2008) 845–854.
- [49] J. Xiao, D. Wang, W. Xu, D. Wang, R.E. Williford, J. Liu, J.G. Zhang, *J. Electrochem. Soc.* 157 (4) (2010) A487–A492.
- [50] L.S. Panchakarla, A. Govindaraj, C.N.R. Rao, *ACS Nano* 1 (2007) 494–500.
- [51] D.C. Higgins, D. Meza, Z. Chen, *J. Phys. Chem. C* 114 (2010) 21982–21988.
- [52] Z. Sheng, L. Shao, J. Chen, W. Bao, F. Wang, X. Xia, *ACS Nano* 5 (6) (2011) 4350–4358.
- [53] S.M. Lyth, Y. Nabae, S. Morlya, S. Kuroki, M. Kakimoto, J. Ozaki, S. Miyata, *J. Phys. Chem. Lett.* 113 (2009) 20148–20151.
- [54] Y. Xia, R. Mokaya, *Chem. Mater.* 17 (2005) 1553–1560.
- [55] N. Alexeyeva, E. Shulga, V. Kisand, I. Kink, K. Tammeveski, *J. Electroanal. Chem.* 648 (2010) 169–175.
- [56] G. Ma, R. Jia, J. Zhao, Z. Wang, C. Song, S. Jia, *J. Phys. Chem. C* 115 (50) (2011) 25148.
- [57] C.V. Rao, C.R. Cabrera, Y. Ishikawa, *J. Phys. Chem. Lett.* 1 (2010) 2622–2627.
- [58] J.D.W. Camacho, K. Stevenson, *J. Phys. Chem. C* 113 (2009) 19082–19090.
- [59] X. Wang, J.S. Lee, Q. Zhu, J. Liu, Y. Wang, S. Dai, *Chem. Mater.* 22 (2010) 2178–2180.
- [60] I.Y. Jeon, D. Yu, S.Y. Bae, H.J. Choi, D.W. Chang, L. Dai, J.B. Baek, *Chem. Mater.* 23 (2011) 3987–3992.
- [61] D.A. Slanac, A. Lie, J.A. Paulson, K.J. Stevenson, K.P. Johnston, *J. Phys. Chem.* 116 (2012) 11032–11039.
- [62] W. Sun, A. Hsu, R. Chen, *J. Power Sources* 196 (2011) 4491–4498.